This paper has been accepted for publication in the AEE journal. This is the version, which has not been fully edited and content may change prior to final publication. Citation information: DOI 10.24425/aee.2026.1991

Improved sensorless scalar control of induction motors using dual RF-MRAS and stator voltage compensation

TAI THANH PHAN[1], **CUONG DINH TRAN**[1*], **MARTIN KUCHAR**[2], **VOJTECH SOTOLA**[2], **PHUONG DUY NGUYEN**[2,3], **KHOA DANG TRAN PHAN**[4], **HUY DUC BUI**[4]

[1]*Power System Optimization Research Group, Faculty of Electrical and Electronics Engineering Ton Duc Thang University Ho Chi Minh City, Vietnam*

[2]*Department of Applied Electronics, Faculty of Electrical Engineering and Computer Science VSB-Technical University of Ostrava Ostrava, Czech Republic*

[3]*Faculty of Engineering and Technology, Saigon University Ho Chi Minh City, Vietnam*

[4]*Faculty of Electrical and Electronics Engineering, Ton Duc Thang University Ho Chi Minh City, Vietnam*

*e-mail: {phanthanhtai/*trandinhcuong/phantrandangkhoa/buiduchuy.st}@tdtu.edu.vn, {martin.kuchar/vojtech.sotola/phuong.nguyen.duy.st}@vsb.cz, phuong.nd@sgu.edu.vn*

Abstract: This paper presents an improved sensorless scalar control (SC) scheme for induction motor drives, aimed at enhancing speed tracking capability in the low-speed region. The proposed method integrates rotor flux-based model reference adaptive system (RF-MRAS) with dual adaptation to estimate both rotor speed and stator resistance. The rotor flux angle obtained from the current model (CM) is used to compute the synchronous speed, while the slip component is filtered before being injected into the scalar frequency command. In addition, a stator-voltage-drop compensation strategy based on estimated stator resistance is introduced to preserve the air-gap flux during low-voltage operation. Simulation studies confirm that the proposed method extends the stable operating range. The minimum stable speeds are 12.23/12.28 rad/s at 20% load, 10.78/11.59 rad/s at 25% load, and 11.88/11.29 rad/s at 30% load, evaluated using $E_{\mathrm{MAPE}}/E_{\max}$ criteria. All cases satisfy $E_{\mathrm{MAPE}} \leq 2\%$ and $E_{\max} \leq 6\%$, showing better low-speed stability than the baseline methods. Laboratory experiments were also performed on an induction motor drive platform. At 300 rpm, online stator resistance estimation strongly reduces speed oscillations under a 20% stator resistance increase. At very low speeds, voltage compensation restores the effective stator voltage and improves steady-state tracking. These results verify that the proposed dual RF-MRAS scheme improves robustness without requiring mechanical speed sensors.

Key words: induction motor, resistance estimation, RF-MRAS, scalar control, sensorless control, voltage compensation

This paper has been accepted for publication in the AEE journal. This is the version, which has not been fully edited and content may change prior to final publication.
Citation information: DOI 10.24425/aee.2026.1991

1. Introduction

Electric machines are widely used in industrial applications due to their robustness and efficiency. Common types include DC motors, permanent magnet synchronous machines, and induction motors [1–3], among which induction motors are the most widely adopted owing to their simple structure, low cost, and high reliability. To achieve high-performance operation, several control techniques have been developed. Field-oriented control (FOC) enables independent regulation of torque and flux with high accuracy and fast response [4–6]. Direct torque control (DTC) directly controls torque and flux, offering fast dynamics and robustness [7, 8]. However, both methods rely on accurate machine models, which increases complexity.

In contrast, scalar control, particularly the constant V/f method, offers a simple, cost-effective solution by maintaining a constant voltage-to-frequency ratio to preserve the air-gap flux [9, 10]. This approach is widely used in applications where high dynamic performance is not required [11, 12]. However, it suffers from limitations in transient response and low-speed operation. Comparative studies in [13] indicate that FOC provides superior dynamic performance, while DTC offers better robustness against parameter variations. Meanwhile, [14] shows that although scalar control exhibits lower performance, it remains attractive due to its simplicity and ease of implementation. In many practical systems, speed measurement is achieved using mechanical sensors such as encoders or tachometers. Although these sensors provide accurate feedback, they increase system cost, reduce reliability, and are susceptible to harsh environmental conditions. Consequently, sensorless control techniques have attracted significant attention as an alternative. Various approaches have been proposed in the literature. Neural network-based methods have demonstrated strong nonlinear approximation capabilities for speed estimation, improving adaptability under varying conditions [15, 16]. Fuzzy logic-based techniques have also been employed to enhance robustness and reduce sensitivity to parameter uncertainties [17, 18].

Model-reference adaptive system (MRAS)-based methods are among the most widely adopted sensorless strategies due to their relatively simple structure and fast convergence. Current-based MRAS (CB-MRAS) uses stator current error for speed estimation and shows improved robustness to parameter mismatches [19, 20]. Reactive power-based MRAS (Q-MRAS) uses reactive power for speed estimation, providing improved performance at low speeds. However, it remains sensitive to variations in machine parameters and may experience stability issues, particularly during regenerative operation [21]. Among various MRAS schemes, rotor flux-based MRAS (RF-MRAS) is widely used for its good estimation performance and compatibility with various control structures, although its accuracy can be affected by parameter variations [22–24]. In addition, sliding mode control (SMC) and sliding mode observers have been introduced to enhance robustness against disturbances and uncertainties, although issues such as chattering remain a challenge [25–27].

A critical issue in sensorless control of induction motor drives is the variation of machine parameters, especially stator resistance. The stator resistance can change significantly with temperature, leading to inaccurate flux and speed estimation, particularly at low speeds [28, 29]. This effect has been further emphasized in [30], where parameter mismatch degrades system

This paper has been accepted for publication in the AEE journal. This is the version, which has not been fully edited and content may change prior to final publication. Citation information: DOI 10.24425/aee.2026.1991

stability. To address this issue, various online estimation techniques have been proposed, including MRAS-based methods [31] and observer-based approaches [32]. However, accurately and stably estimating stator resistance under varying operating conditions remains a challenging problem. In scalar-controlled drives, another major limitation arises from the stator resistive voltage drop at low frequencies. As the stator voltage decreases with frequency, the voltage drop across stator resistance becomes dominant, resulting in flux weakening and reduced torque capability. To mitigate this issue, various compensation techniques have been proposed, including voltage-boost methods, vector compensation, and flux-based compensation schemes [33, 34]. Nevertheless, these methods often suffer from overcompensation, increased complexity, or limited effectiveness under varying load conditions.

Despite the extensive research efforts, several limitations persist. High-performance methods such as FOC and DTC offer excellent dynamic characteristics but require complex structures and accurate parameter knowledge. Scalar control, on the other hand, remains attractive due to its simplicity but suffers from poor performance at low speeds and limited robustness. Existing sensorless techniques, particularly MRAS-based methods, have shown promising results; however, most studies focus on speed estimation alone and do not simultaneously address parameter variation and low-speed performance degradation. Furthermore, stator resistance variation and stator voltage drop compensation are often treated separately, leading to suboptimal system performance. A unified approach that integrates robust speed estimation, parameter adaptation, and low-speed compensation within a simple scalar control framework is still lacking. A summary of representative control methods and their key features is presented in Table 1.

Table 1. Summary of control approaches for induction motor drives and key features

Ref.	**Speed estimation**	**R_s estimation**	**Stator voltage compensation**	**Control method**	**Contribution**
[9]	Yes (ANN-based)	No	No	Scalar control	Introduces an ANN-based speed estimator using stator voltage and current signals.
[12]	Yes (MRAS-based)	No	No		Comparative evaluation of VF-MRAS and FOC-MRAS for induction motor drives under different load conditions.
[24]	Yes (Flux-based slip estimation)	No	No		Improves speed control performance under load disturbances using a discrete-time flux observer.
[29]	No	Yes (PQ-MRAS-based)	No	Vector control	Simultaneous estimation of stator and rotor resistances using active and reactive power.
[32]	Yes	Yes	No		Robust online stator resistance estimation ensures accurate speed estimation at low speeds.

This paper has been accepted for publication in the AEE journal. This is the version, which has not been fully edited and content may change prior to final publication.
Citation information: DOI 10.24425/aee.2026.1991

	(MRAS-based speed estimation)	(MRAS stator resistance identification)			
[33]	Yes (Slip estimation)	No	Yes (voltage drop compensation)	Scalar control	Compensation of slip frequency and stator voltage drop to improve low-frequency operation.
[34]	Yes (Flux-based estimation)	No	Yes (flux compensation)		Enhances torque capability and low-speed regulation without an encoder.
Proposed Method	Yes (RF-MRAS-based)	Yes (RF-MRAS-based)	Yes (voltage drop compensation)		Simultaneous rotor speed estimation, stator resistance adaptation, and voltage-drop compensation within the scalar control framework.

As shown in Table 1, several studies focus on speed estimation without addressing stator resistance variation or voltage drop compensation [9, 12, 24]. Meanwhile, some works consider stator resistance estimation using MRAS-based approaches, but are mainly applied within vector control frameworks such as FOC [29, 32]. On the other hand, scalar control-based studies incorporate stator-voltage-drop compensation to improve low-speed performance but typically neglect stator-resistance variation [33, 34]. Therefore, a unified approach integrating speed estimation, resistance adaptation, and voltage compensation remains necessary.

This paper proposes an improved sensorless scalar control scheme for induction motor drives operating in the low-speed region. The method combines rotor-flux-based MRAS with a dual-adaptation mechanism to estimate both rotor speed and stator resistance in a unified structure. The rotor flux is obtained from the current model, and the synchronous speed is derived from the flux angle to calculate the slip component. A first-order filter is then applied to suppress high-frequency ripple in the slip signal. To overcome flux weakening at low frequency, a stator resistance voltage drop compensation strategy is also introduced. This preserves the air gap flux and improves torque capability without increasing the complexity of conventional scalar control.

2. Mathematical model of the three-phase induction motor

To develop the proposed sensorless scalar control scheme, an accurate mathematical model of the induction motor is first established in the stationary (α, β) reference frame [35]. Under standard assumptions (linear magnetic circuit, negligible core losses), the dynamic behavior of the induction motor can be described by the following equations:

$$i_{s\alpha} = Z_1 \int \left(\frac{u_{s\alpha}}{L_m} - \frac{R_s i_{s\alpha}}{L_m} + \frac{L_m \omega_r i_{s\beta}}{L_r} + \frac{R_r i_{r\alpha}}{L_r} + \omega_r i_{r\beta} \right) \mathrm{d}t, \tag{1}$$

$$i_{s\beta} = Z_1 \int \left(\frac{u_{s\beta}}{L_m} - \frac{L_m \omega_r i_{s\alpha}}{L_r} - \frac{R_s i_{s\beta}}{L_m} - \omega_r i_{r\alpha} + \frac{R_r i_{r\beta}}{L_r} \right) \mathrm{d}t, \tag{2}$$

This paper has been accepted for publication in the AEE journal. This is the version, which has not been fully edited and content may change prior to final publication.
Citation information: DOI 10.24425/aee.2026.1991

$$i_{r\alpha} = Z_2 \int \left(\frac{u_{s\alpha}}{L_s} - \frac{R_s i_{s\alpha}}{L_s} + \omega_r i_{s\beta} + \frac{R_r i_{r\alpha}}{L_m} + \frac{L_r \omega_r i_{r\beta}}{L_m}\right) \mathrm{d}t, \tag{3}$$

$$i_{r\beta} = Z_2 \int \left(\frac{u_{s\beta}}{L_s} - \omega_r i_{s\alpha} - \frac{R_s i_{s\beta}}{L_s} - \frac{L_r \omega_r i_{r\alpha}}{L_m} + \frac{R_r i_{r\beta}}{L_m}\right) \mathrm{d}t. \tag{4}$$

Here,

$$Z_1 = (L_m L_r)/(L_s L_r - L_m^2), \quad Z_2 = (L_s L_m / L_m^2 - L_s L_r),$$

where $u_{s\alpha}$, $i_{s\alpha}$, and $i_{r\alpha}$ denote the stator voltage, stator current, and rotor current along the α-axis. $u_{s\beta}$, $i_{s\beta}$, and $i_{r\beta}$ denote the stator voltage, stator current, and rotor current along the β-axis. R_s, R_r are the stator and rotor resistances, while L_s, L_r, and L_m represent the stator, rotor, and magnetizing inductances. The rotor angular speed is denoted by ω_r.

The mechanical dynamics of the motor are governed by the torque balance equation [36]:

$$T_e = T_L + \frac{J}{p}\frac{\mathrm{d}\omega_r}{\mathrm{d}t} = T_L + J\frac{\mathrm{d}\omega_m}{\mathrm{d}t}. \tag{5}$$

J is the motor inertia, T_L is the load torque, T_e is the electromagnetic torque, p is the number of pole pairs. The mechanical angular speed is denoted by $\omega_m = \omega_r/p$.

3. Design of the RF-MRAS speed and stator resistance estimator

The RF-MRAS scheme comprises two main components: a reference model and an adaptive model [37]. The reference model is constructed using the stator voltage equations, where the rotor flux is obtained without involving the rotor speed. It can be expressed as follows:

$$\psi_{r\alpha}^{RM} = \frac{L_r}{L_m}\left[\int (u_{s\alpha} - \hat{R}_s i_{s\alpha})\mathrm{d}t - \frac{L_s L_r - L_m^2}{L_r} i_{s\alpha}\right], \tag{6}$$

$$\psi_{r\beta}^{RM} = \frac{L_r}{L_m}\left[\int (u_{s\beta} - \hat{R}_s i_{s\beta})\mathrm{d}t - \frac{L_s L_r - L_m^2}{L_r} i_{s\beta}\right], \tag{7}$$

where $\psi_{r\alpha}^{RM}$ and $\psi_{r\beta}^{RM}$ are the rotor flux components from the reference model in the stationary (α, β) reference and $\hat{R}_s$ is the estimated stator resistance from RF-MRAS. In contrast, the adaptive model is derived from the rotor circuit equations, where the rotor speed explicitly appears. The rotor flux components estimated by the adaptive model are given by:

$$\psi_{r\alpha}^{AM} = \int \left(\frac{L_m \times R_r}{L_r} i_{s\alpha} - \frac{R_r}{L_r}\psi_{r\alpha}^{AM} - \hat{\omega}_r \psi_{r\beta}^{AM}\right)\mathrm{d}t, \tag{8}$$

$$\psi_{r\beta}^{AM} = \int \left(\frac{L_m \times R_r}{L_r} i_{s\beta} - \frac{R_r}{L_r}\psi_{r\beta}^{AM} + \hat{\omega}_r \psi_{r\alpha}^{AM}\right)\mathrm{d}t, \tag{9}$$

where $\psi_{r\alpha}^{AM}$ and $\psi_{r\beta}^{AM}$ are the rotor flux components from the adaptive model in the stationary (α, β) reference, and $\hat{\omega}_r$ is the estimated rotor angular speed from RF-MRAS.

The core principle of MRAS is to minimize the deviation between the outputs of the reference and adaptive models. The rotor flux deviation for speed estimation is defined in Eq. (10).

This paper has been accepted for publication in the AEE journal. This is the version, which has not been fully edited and content may change prior to final publication. Citation information: DOI 10.24425/aee.2026.1991

$$\xi_\omega = (\psi_{r\alpha}^{AM}\psi_{r\beta}^{RM}) - (\psi_{r\beta}^{AM}\psi_{r\alpha}^{RM}). \tag{10}$$

This mismatch signal is used to drive a proportional-integral (PI) adaptation mechanism to estimate the rotor speed:

$$\widehat{\omega}_r = K_{p,\omega}(\xi_\omega + K_{i,\omega}\int \xi_\omega \mathrm{d}t), \tag{11}$$

where $K_{p,\omega}$ and $K_{i,\omega}$ are the proportional and integral gains of the speed adaptation mechanism. The estimated speed is continuously adjusted such that the rotor fluxes from both models converge.

The stator resistance adaptation is based on the projection of the rotor flux error onto the stator current components, defined as:

$$\xi_{R_s} = (\psi_{r\alpha}^{RM} - \psi_{r\alpha}^{AM})i_{s\alpha} + (\psi_{r\beta}^{RM} - \psi_{r\beta}^{AM})i_{s\beta}. \tag{12}$$

The estimated stator resistance is updated using another PI adaptation law:

$$\hat{R}_s = K_{p,R_s}(\xi_{R_s} + K_{i,R_s}\int \xi_{R_s}\mathrm{d}t), \tag{13}$$

where K_{p,R_s} and K_{i,R_s} are the proportional and integral gains of the stator resistance adaptation mechanism, respectively. The overall RF-MRAS structure, including both adaptation loops for rotor speed and stator resistance, is illustrated in Fig. 1. The adaptation mechanism enables simultaneous estimation of the rotor speed and identification of the stator resistance.

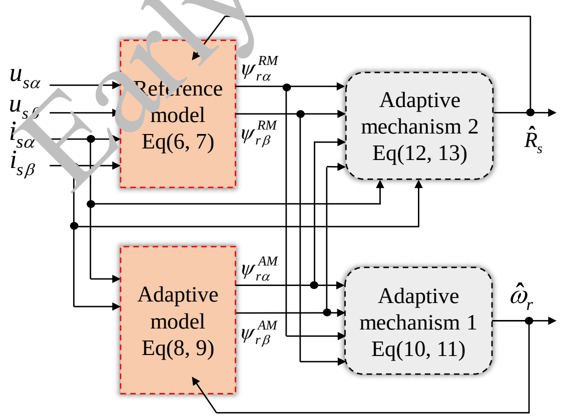

Fig. 1. RF-MRAS scheme for rotor speed and stator resistance estimation

4. Slip compensation and stator resistance voltage drop compensation

In this study, the rotor flux angle is calculated from the adaptive model (current model) rather than the voltage model, since the current model generally provides better robustness in low-

This paper has been accepted for publication in the AEE journal. This is the version, which has not been fully edited and content may change prior to final publication.
Citation information: DOI 10.24425/aee.2026.1991

speed operation and is less sensitive to pure integration problems. The issue of integral drift is addressed in research [38]. Accordingly, the rotor flux angle is expressed as

$$\theta_{\psi r} = \tan^{-1}\left(\psi_{r\beta}^{AM} / \psi_{r\alpha}^{AM}\right), \tag{14}$$

where $\theta_{\psi r}$ is the rotor flux angle. The synchronous speed is then obtained from the time derivative of the rotor flux angle.

$$\omega_e = \mathrm{d}\theta_{\psi_r} / \mathrm{d}t. \tag{15}$$

The slip speed is determined from the deviation between the synchronous speed and the estimated rotor speed as

$$\omega_{\text{slip}} = (\omega_e - \widehat{\omega}_r)/p, \tag{16}$$

where ω_{slip} is the slip angular speed. Since the computed slip signal may contain high-frequency ripple, a first-order low-pass filter is introduced to smooth the slip component before it is used in the scalar control loop.

$$G_{f(s)} = \frac{10}{s+10}, \tag{17}$$

where, $G_{f(s)}$ is the slip filter transfer function, and the cutoff angular frequency is ω_f.

In this work, the filter time constant is chosen as $\tau = 0.1$ s, which corresponds to $\omega_f = 10$ rad/s. The cutoff frequency is selected according to $\omega_f \approx 1/T_r$, where T_r is the rotor time constant. With $L_r = 0.209$ H and $R_r = 2.118\ \Omega$, the rotor time constant $T_r = L_r / R_r = 0.09867$ s.

In the digital implementation, the rotor flux angle is computed using $\text{atan2}(\psi_{r\beta}^{AM}, \psi_{r\alpha}^{AM})$ and unwrapped to avoid discontinuities at $\pm\pi$. The synchronous speed is then obtained by a backward Euler finite difference, $\omega_e[k] = (\theta_{\psi r}[k] - \theta_{\psi r}[k-1])/T_s$, with $T_s = 1 \times 10^{-5}$ s.

The filtered slip speed is therefore written as

$$\omega_{\text{slip}}^{f}(\mathrm{s}) = G_f(\mathrm{s})\omega_{\text{slip}}(\mathrm{s}), \tag{18}$$

where ω_{slip}^{f} is the filtered slip speed. The slip speed filtering scheme is illustrated in Fig. 2. Based on Fig. 3, a smaller filter time constant ($\tau = 0.0333$ s) results in increased overshoot and oscillations, while a larger value ($\tau = 0.3$ s) slows the transient response. Therefore, $\tau = 0.1$ s provides a balanced trade-off between dynamic performance and noise attenuation.

The classical scalar control relationship is given by:

$$\frac{V_{e,\text{RMS}}}{f} = 4.44.N.|\psi_s|.\delta \Rightarrow \frac{V}{f} = \text{constant}, \tag{19}$$

where: $V_{e,\text{RMS}}$ is the RMS stator voltage, f is the supply frequency, N is the number of turns, $|\psi_s|$ is the magnitude of the stator flux linkage vector, and δ is the waveform factor.

This paper has been accepted for publication in the AEE journal. This is the version, which has not been fully edited and content may change prior to final publication.
Citation information: DOI 10.24425/aee.2026.1991

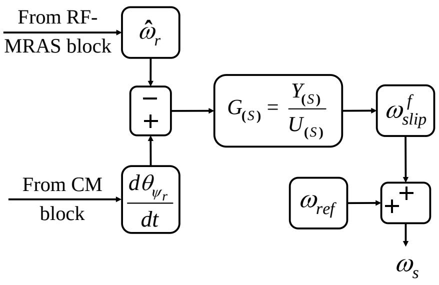

Fig. 2. Slip speed filtering scheme using a first-order low-pass filter

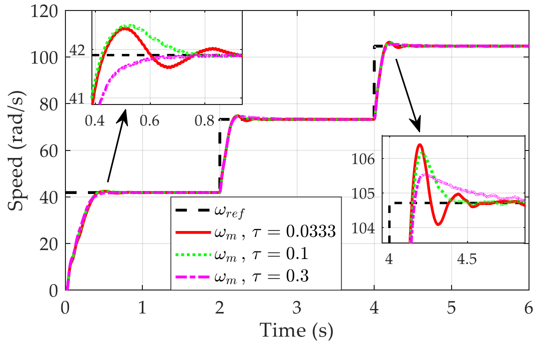

Fig. 3. Effect of filter time constant on motor speed response

At low speeds, the stator voltage is small. The resistive voltage drop becomes significant compared to the applied voltage. As a result, the actual flux decreases, which leads to degraded torque performance. Therefore, the proposed method introduces a compensation term for stator resistance voltage drop.

The compensated stator voltage reference is expressed as

$$V_s^* = \frac{V_{\text{rated}}}{f_{\text{rated}}}.f^* + \Delta V_{R_s} = \frac{V_{\text{rated}}}{\omega_{e,\text{rated}}} p.(\omega^* + \omega_{\text{slip}}^f) + \hat{R}_s.I_s, \tag{20}$$

where: V_s^* is the compensated stator voltage reference, V_{rated} is the rated stator voltage, f_{rated} is the rated frequency, $\omega_{e,\text{rated}}$ is the rated synchronous angular speed, ω^* is the reference mechanical speed, and $I_s = \sqrt{i_{s\alpha}^2 + i_{s\beta}^2}$ is the stator current magnitude.

The stator resistance voltage drop compensation is limited to 10% of the rated voltage, as mentioned in Eq. (21):

$$\Delta V_{R_s} = \min(\hat{R}_s I_s, 0.1 V_{\text{rated}}). \tag{21}$$

The maximum voltage compensation is set to 10% V_{rated} as a compromise between low speed stability and current limitation. A lower limit provides insufficient compensation for the stator resistance voltage drop, whereas a higher limit may increase the stator current close to, or beyond, the rated current of the motor. The overall structure of the proposed sensorless scalar control scheme based on RF-MRAS is illustrated in Fig. 4.

This paper has been accepted for publication in the AEE journal. This is the version, which has not been fully edited and content may change prior to final publication. Citation information: DOI 10.24425/aee.2026.1991

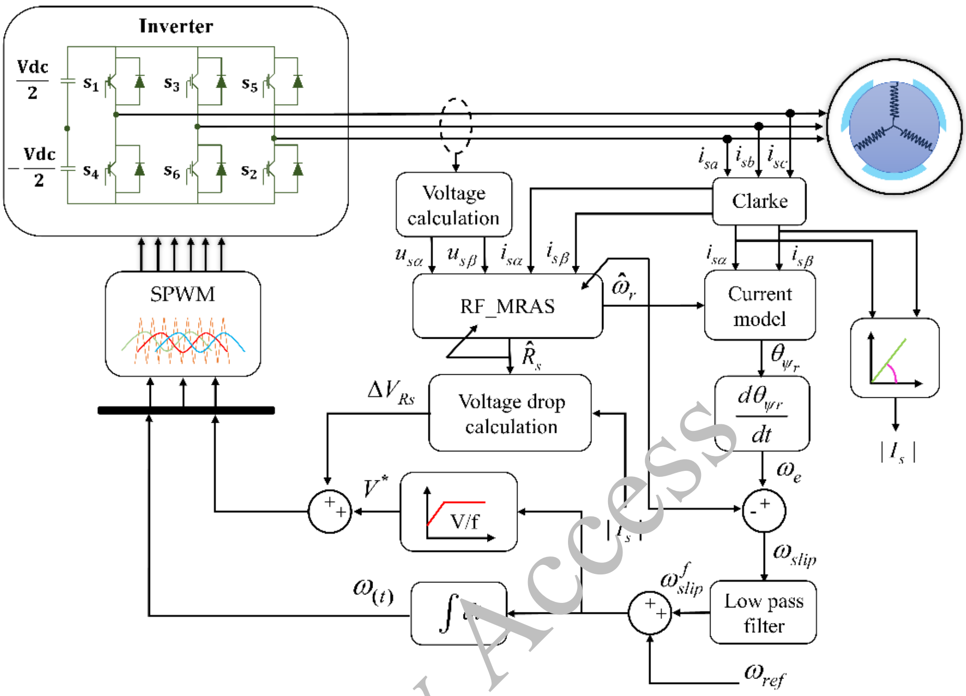

Fig. 4. Proposed RF-MRAS-based sensorless scalar control scheme for induction motor drives

5. Local stability analysis of the RF-MRAS adaptation mechanism

This section analyzes the local stability properties of the proposed dual RF-MRAS adaptation mechanism. The objective is to establish the boundedness of the RF-MRAS estimation errors and to clarify the conditions under which the rotor-speed and stator-resistance estimation errors can converge.

The magnetic flux vectors of the reference model and the adaptive model are represented as matrices:

$$\boldsymbol{\Psi}_r^{RM} = \begin{bmatrix} \psi_{r\alpha}^{RM} \\ \psi_{r\beta}^{RM} \end{bmatrix}, \quad \boldsymbol{\Psi}_r^{AM} = \begin{bmatrix} \psi_{r\alpha}^{AM} \\ \psi_{r\beta}^{AM} \end{bmatrix}. \tag{22}$$

The mismatch between these two vectors represents the rotor-flux estimation deviation.

$$\tilde{\boldsymbol{\Psi}}_r = \boldsymbol{\Psi}_r^{RM} - \boldsymbol{\Psi}_r^{AM}. \tag{23}$$

The parameter estimation errors are written as $\tilde{\omega}_r = \omega_r - \hat{\omega}_r$, $\tilde{R}_s = R_s - \hat{R}_s$. From Eqs. (6), (7), (8), and (9), reference and adaptive rotor flux dynamics can be expressed in the form

This paper has been accepted for publication in the AEE journal. This is the version, which has not been fully edited and content may change prior to final publication. Citation information: DOI 10.24425/aee.2026.1991

$$\dot{\boldsymbol{\psi}}_{\boldsymbol{r}}^{\boldsymbol{RM}} = f_{RM}(\boldsymbol{\psi}_{\boldsymbol{r}}^{\boldsymbol{RM}}, \boldsymbol{i_s}, \boldsymbol{u_s}, \hat{R}_s), \tag{24}$$

$$\dot{\boldsymbol{\psi}}_{\boldsymbol{r}}^{\boldsymbol{AM}} = f_{AM}(\boldsymbol{\psi}_{\boldsymbol{r}}^{\boldsymbol{AM}}, \boldsymbol{i_s}, \hat{\omega}_r). \tag{25}$$

Differentiating Eq. (23) gives

$$\dot{\tilde{\boldsymbol{\psi}}}_{\boldsymbol{r}} = \dot{\boldsymbol{\psi}}_{\boldsymbol{r}}^{\boldsymbol{RM}} - \dot{\boldsymbol{\psi}}_{\boldsymbol{r}}^{\boldsymbol{AM}}. \tag{26}$$

Substituting the model expressions (24), (25) into (26) results in a differential equation describing the evolution of the flux estimation error.

$$\dot{\tilde{\boldsymbol{\psi}}}_{\boldsymbol{r}} = \boldsymbol{A}\tilde{\boldsymbol{\psi}}_{\boldsymbol{r}} + \boldsymbol{W_w}(t)\tilde{\omega}_r + \boldsymbol{W_R}(t)\tilde{R}_s, \tag{27}$$

where

$$\boldsymbol{A} = \begin{bmatrix} -1/T_r & -\omega_r \\ \omega_r & -1/T_r \end{bmatrix}, \qquad T_r = \frac{L_r}{R_r} > 0. \tag{28}$$

The matrix $\boldsymbol{A}$ describes the intrinsic rotor-flux-error dynamics when the estimated parameters equal their actual values. Since $T_r > 0$, the symmetric part of $\boldsymbol{A}$ is negative definite:

$$\frac{\boldsymbol{A}+\boldsymbol{A}^{\boldsymbol{T}}}{2} = -\frac{1}{T_r}\boldsymbol{I}. \tag{29}$$

Thus, the nominal flux error dynamics are exponentially stable. The speed estimation error enters the adaptive model through the rotational coupling between the two rotor flux axes. Using the skew-symmetric matrix

$$\boldsymbol{J} = \begin{bmatrix} 0 & -1 \\ 1 & 0 \end{bmatrix}, \qquad \boldsymbol{J}^{\boldsymbol{T}} = -\boldsymbol{J}. \tag{30}$$

The speed-related and resistance-related regressors can be written as

$$\boldsymbol{W_\omega}(t) = \boldsymbol{J}\boldsymbol{\psi}_{\boldsymbol{r}}^{\boldsymbol{AM}}, \quad \boldsymbol{W_R}(t) = \Gamma_R \boldsymbol{i_s}, \tag{31}$$

where Γ_R is a constant coefficient determined by the induction motor parameters and by the adopted rotor flux reference model. Substituting (31) into (27), the local flux error dynamics become

$$\dot{\tilde{\boldsymbol{\psi}}}_{\boldsymbol{r}} = \boldsymbol{A}\tilde{\boldsymbol{\psi}}_{\boldsymbol{r}} + \boldsymbol{J}\boldsymbol{\psi}_{\boldsymbol{r}}^{\boldsymbol{AM}}\tilde{\omega}_r + \Gamma_R \boldsymbol{i_s}\tilde{R}_s. \tag{32}$$

Since both errors affect the same flux error dynamics, simultaneous convergence of $\tilde{\omega}_r$ and $\tilde{R}_s$ cannot be guaranteed without sufficient excitation of the corresponding regressors.

The two adaptation signals used in the RF-MRAS can be expressed as

$$\xi_\omega = \tilde{\boldsymbol{\psi}}_{\boldsymbol{r}}^{\boldsymbol{T}}\boldsymbol{J}\boldsymbol{\psi}_{\boldsymbol{r}}^{\boldsymbol{AM}}, \tag{33}$$

$$\xi_R = \tilde{\boldsymbol{\psi}}_{\boldsymbol{r}}^{\boldsymbol{T}}\boldsymbol{i_s}. \tag{34}$$

For stability analysis, the following integral adaptation laws are considered:

This paper has been accepted for publication in the AEE journal. This is the version, which has not been fully edited and content may change prior to final publication.
Citation information: DOI 10.24425/aee.2026.1991

$$\dot{\hat{\omega}}_r = \gamma_\omega \boldsymbol{\tilde{\psi}_r^T J \psi_r^{AM}}, \tag{35}$$

$$\dot{\hat{R}}_s = \gamma_R \Gamma_R \boldsymbol{\tilde{\psi}_r^T i_s}, \tag{36}$$

where $\gamma_\omega > 0$ and $\gamma_R > 0$ are positive adaptation gains. In practical implementation, proportional terms may be added to improve the transient response. However, the Lyapunov analysis below is established for the integral part of the adaptation laws. Consider the Lyapunov candidate function

$$V = \frac{1}{2}\boldsymbol{\tilde{\psi}_r^T \tilde{\psi}_r} + \frac{1}{2\gamma_\omega}\tilde{\omega}_r^2 + \frac{1}{2\gamma_R}\tilde{R}_s^2. \tag{37}$$

Since $\gamma_\omega > 0$ and $\gamma_R > 0$, V is positive definite with respect to $\boldsymbol{\tilde{\psi}_r}$, $\tilde{\omega}_r$, and $\tilde{R}_s$. Assuming that the actual rotor speed and stator resistance are constant or slowly varying during the adaptation interval, one has

$$\dot{\tilde{\omega}}_r = -\dot{\hat{\omega}}_r, \dot{\tilde{R}}_s = -\dot{\hat{R}}_s. \tag{38}$$

Taking the time derivative of (37) yields

$$\dot{V} = \boldsymbol{\tilde{\psi}_r^T \dot{\tilde{\psi}}_r} + \frac{1}{\gamma_\omega}\tilde{\omega}_r \dot{\tilde{\omega}}_r + \frac{1}{\gamma_R}\tilde{R}_s \dot{\tilde{R}}_s. \tag{39}$$

Substituting (32), (35), and (36) into (39) gives

$$\dot{V} = \boldsymbol{\tilde{\psi}_r^T A \tilde{\psi}_r} + \boldsymbol{\tilde{\psi}_r^T J \psi_r^{AM}}\tilde{\omega}_r + \Gamma_R \boldsymbol{\tilde{\psi}_r^T i_s}\tilde{R}_s - \tilde{\omega}_r \boldsymbol{\tilde{\psi}_r^T J \psi_r^{AM}} - \Gamma_R \tilde{R}_s \boldsymbol{\tilde{\psi}_r^T i_s}. \tag{40}$$

The cross-coupling terms associated with $\tilde{\omega}_r$and $\tilde{R}_s$ are cancelled by the adaptation laws. Therefore,

$$\dot{V} = \boldsymbol{\tilde{\psi}_r^T A \tilde{\psi}_r}. \tag{41}$$

Using (29), one obtains

$$\dot{V} = -\frac{1}{T_r}\boldsymbol{\tilde{\psi}_r^T \tilde{\psi}_r} \le 0. \tag{42}$$

Therefore, the Lyapunov function is non-increasing. This result implies that $\boldsymbol{\tilde{\psi}_r}$, $\tilde{\omega}_r$, and $\tilde{R}_s$ are bounded for bounded initial conditions. Moreover,

$$\int_0^\infty \left\|\boldsymbol{\tilde{\psi}_r}(t)\right\|^2 \mathrm{d}t < \infty, \tag{43}$$

which means that the flux estimation error is square-integrable. If the measured stator currents, rotor flux estimates, and machine speed remain bounded, then $\boldsymbol{\dot{\tilde{\psi}}_r}$ is also bounded. Under this condition, Barbalat's lemma gives

$$\lim_{t\to\infty}\boldsymbol{\tilde{\psi}_r}(t) = 0. \tag{44}$$

Thus, the RF-MRAS adaptation mechanism guarantees bounded estimation errors and convergence of the rotor flux error under bounded operating conditions. However, convergence

This paper has been accepted for publication in the AEE journal. This is the version, which has not been fully edited and content may change prior to final publication. Citation information: DOI 10.24425/aee.2026.1991

of the flux estimation error does not automatically imply convergence of both parameter estimation errors. From (32), when $\tilde{\boldsymbol{\psi}}_{\boldsymbol{r}} \to 0$, the remaining parameter dependent term is governed by the regressor matrix

$$\boldsymbol{\Phi}(t) = [\boldsymbol{J}\boldsymbol{\psi}_{\boldsymbol{r}}^{\boldsymbol{AM}} \Gamma_R \boldsymbol{i}_{\boldsymbol{s}}], \tag{45}$$

with the parameter error vector

$$\tilde{\boldsymbol{\theta}} = \begin{bmatrix} \tilde{\omega}_r \\ \tilde{R}_s \end{bmatrix}. \tag{46}$$

Parameter errors can converge only if the regressor matrix is sufficiently informative. A standard sufficient condition is the persistent excitation condition: there exist positive constants $T_0 > 0$ and $\alpha > 0$ such that

$$\int_t^{t+T_0} \boldsymbol{\Phi}^{\boldsymbol{T}}(\tau)\boldsymbol{\Phi}(\tau)\mathrm{d}\tau \geq \alpha\boldsymbol{I}, \quad \forall t \geq 0. \tag{47}$$

If (47) is satisfied, the two parameter error components are distinguishable, and the estimation errors $\tilde{\omega}_{\boldsymbol{r}}$ and $\tilde{R}_s$ can converge to zero. If this condition is not satisfied, the analysis only guarantees boundedness of the parameter errors and convergence of the flux estimation error. The estimated stator resistance is constrained within a feasible range:

$$R_{s,\min} \leq \hat{R}_s \leq R_{s,\max}, \tag{48}$$

where $R_{s,\min} > 0$ and $R_{s,\max}$ are selected as twice the nominal stator resistance.

Consequently, the proposed dual RF-MRAS mechanism establishes local boundedness and convergence of the rotor flux error under bounded operating conditions. Asymptotic convergence of both rotor speed and stator resistance estimation errors is conditional and requires sufficient excitation of the flux and current regressors. Therefore, the proposed estimator is regarded as a locally stable adaptive mechanism within a bounded operating region.

The PI gains used in the RF-MRAS adaptation loops are listed: $K_{p,\omega} = 100$, $K_{i,\omega} = 10\,000$, $K_{p,Rs} = 10$ and $K_{i,Rs} = 100$. Using the ideal PI relation $K_i = K_p/T_i$. So $T_{i,\omega} = K_{p,\omega}/K_{i,\omega} = 100/10\,000 = 0.01$ and $T_{i,Rs} = K_{p,Rs}/K_{i,Rs} = 10/100 = 0.1$. Following the practical Routh-Hurwitz-based tuning procedure in [39], each adaptation loop is locally approximated by

$$G_x(s) = \frac{1}{T_x s + 1}, \quad C_x(s) = K_{p,x}\left(1 + \frac{1}{T_{i,x}s}\right). \tag{49}$$

The characteristic equation is

$$D_x(s) = T_{i,x}T_x s^2 + T_{i,x}(1 + K_{p,x})s + K_{p,x}. \tag{50}$$

For $T_x = 0.2$, the speed loop gives $s_{\omega,1} = -135.21$, $s_{\omega,2} = -369.79$, while the stator resistance loop gives $s_{R_s,1} = -11.49$, $s_{R_{s,2}} = -43.51$. Hence, all poles lie in the left half plane.

This paper has been accepted for publication in the AEE journal. This is the version, which has not been fully edited and content may change prior to final publication.
Citation information: DOI 10.24425/aee.2026.1991

6. Simulation results

A set of simulation studies was carried out on a three-phase induction motor drive using the machine parameters listed in Table 2.

Table 2. Induction motor parameters used in the simulation study

Parameter	**Value**	**Unit**	**Parameter**	**Value**	**Unit**
Rated Power: P_{rated}	2 200	W	Rotor inductance: L_r	0.209	H
Rated frequency: f_{rated}	50	Hz	Magnetizing inductance: L_m	0.192	H
Stator resistance: R_s	3.179	Ω	Motor inertia: J	0.0047	kg.m^2
Rotor resistance: R_r	2.118	Ω	Rated torque: T_{rated}	14.8	N.m
Stator inductance: L_s	0.209	H	Pole pair: p	2	---

Three simulation methods are defined to isolate the contribution of each proposed component. The methods can be summarized as: Method 0 - M0 (without R_s estimation or compensation); Method 1 - M1 (with R_s estimation only); and Method 2 - M2 (with both R_s estimation and compensation). Based on these methods, five simulation scenarios are designed, with scenario 5 comparing all methods in the low-speed region to determine the minimum stable operating speed, evaluated using mean absolute percentage error (MAPE) and maximum absolute percentage error. The MAPE is defined as

$$E_{\text{MAPE}}(\%) = \frac{1}{N}\sum_{k=1}^{N}\left|\frac{\omega_{\text{ref}}(k)-\omega_m(k)}{\omega_{\text{ref}}(k)}\right|.100, \tag{51}$$

where: N is the number of samples, $\omega_{\text{ref}}(k)$ is the reference speed, and $\omega_m(k)$ is the measured motor speed at the k-th sampling instant. The maximum absolute percentage error is defined

$$E_{\max}(\%) = \max_{1\le k\le N}\left(\left|\frac{\omega_{\text{ref}}(k)-\omega_m(k)}{\omega_{\mathbf{ref}}(k)}\right|\right).100, \tag{52}$$

where $E_{\max}$ represents the worst-case deviation over the entire observation interval.

The metric E_{MAPE} reflects the average tracking performance over time and is therefore used to assess the steady-state accuracy and long-term stability of the system. In contrast, $E_{\max}$ captures the peak deviation and is particularly useful for detecting short-duration disturbances, transient spikes, or fluctuations that may not be reflected in the average error. In this study, a speed operating point is considered stable if both conditions $E_{\text{MAPE}} \le 2\%$ and $E_{\max} \le 6\%$ are satisfied. The simulation scenarios considered in this study are summarized in Table 3.

Table 3. Summary of simulation scenarios

This paper has been accepted for publication in the AEE journal. This is the version, which has not been fully edited and content may change prior to final publication. Citation information: DOI 10.24425/aee.2026.1991

Scenario	Purpose	Compared method
1	Effect of stator resistance variation on speed response	M0–M1
2	Effect of stator resistance voltage drop at very low speed	M1–M2
3	Effect of gradual stator resistance variation and stator resistance voltage drop at very low speed	M2
4	Performance under a wide-range speed reference profile	M2
5	Investigation of minimum stable operating speed	M0–M1–M2

Scenario 1: Effect of stator resistance variation

Scenario 1 evaluates the impact of stator resistance variation on speed estimation and control performance, with emphasis on the role of R_s adaptation. The reference speed is ramped to 31.5 rad/s within 0.5 s and then maintained. At t = 3 s, the stator resistance is increased by 30%, introducing a parameter mismatch. In Method 0 (M0), where R_s is fixed (Fig. 5(c)), the reference model becomes inaccurate. This mismatch propagates to rotor flux estimation, leading to oscillations and deviation in the estimated speed, as observed in Fig. 5(a). The instability indicates RF-MRAS's sensitivity to parameter variations without adaptation. This effect is also reflected in the slip response (Fig. 5(b)). After the resistance change, the slip increases from approximately 1.2 rad/s to around 1.7 rad/s, showing that the controller attempts to compensate for flux degradation, albeit inaccurately due to incorrect parameter knowledge.

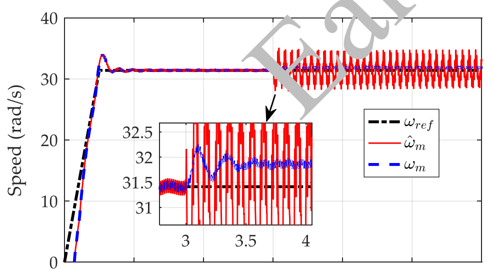

(a)

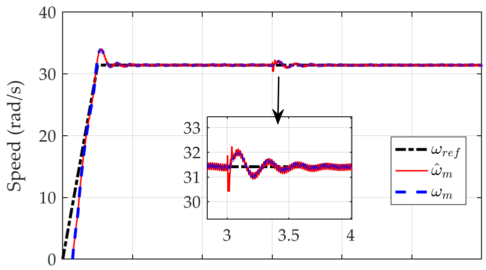

(a)

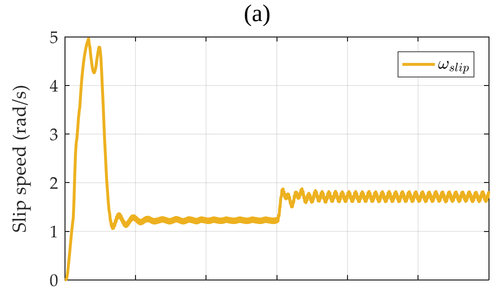

(b)

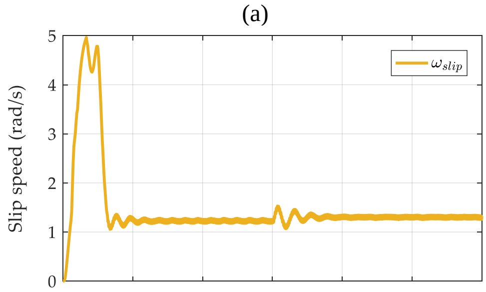

(b)

This paper has been accepted for publication in the AEE journal. This is the version, which has not been fully edited and content may change prior to final publication.
Citation information: DOI 10.24425/aee.2026.1991

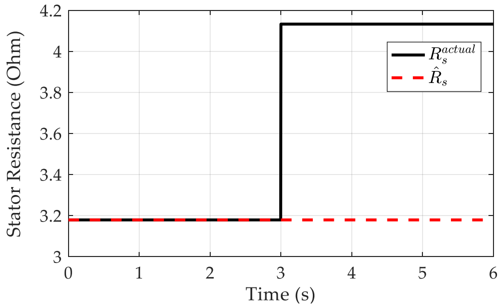

(c)

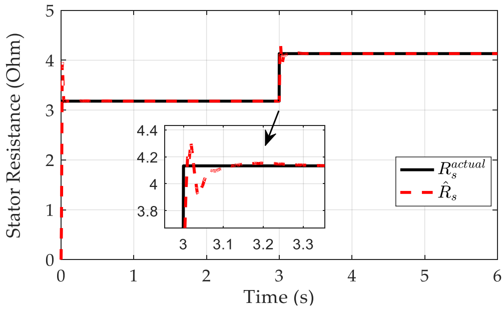

(c)

Fig. 5. The results with Method 0 in Scenario 1: (a) speed response; (b) slip speed response; (c) stator resistance response

Fig. 6.The results with Method 1 in Scenario 1: (a) speed response; (b) slip speed response; (c) stator resistance response

In contrast, Method 1 (M1) incorporates online R_s estimation. As shown in Fig. 6(c), the estimated resistance rapidly converges to the new value, ensuring consistency in the reference model. Consequently, the speed response (Fig. 6(a)) remains stable, with only minor transient oscillations, and quickly recovers. Similarly, the slip response (Fig. 6(b)) exhibits improved stability with minimal disturbance. These results demonstrate that R_s estimation significantly enhances robustness against parameter variations. However, since this scenario is conducted at moderate speed, the influence of stator voltage drop is limited, motivating further analysis at very low speeds in Scenario 2.

Scenario 2: Effect of stator resistance voltage drop at very low speed

Scenario 2 evaluates system performance in the very low-speed region (around 10% rated speed), where the stator voltage is small, and the resistive voltage drop becomes dominant, a key limitation of conventional scalar control. Both methods (M1 and M2) include R_s estimation, with a 30% increase in stator resistance at t = 3 s (Figs. 7(c) and 8(c)). In M1, although R_s is accurately estimated (Fig. 7(c)), the speed response (Fig. 7(a)) exhibits significant oscillations and overshoot. The slip response (Fig. 7(b)) also shows persistent oscillations. This occurs because the stator voltage drop is not compensated, resulting in reduced effective stator voltage and underestimation of flux. Consequently, rotor flux estimation becomes inaccurate, resulting in unstable speed and slip behavior.

In contrast, M2 incorporates both R_s estimation and voltage drop compensation. The compensation term (Fig. 8(d)) adapts in real time based on the estimated R_s and stator current. By restoring the effective stator voltage, the desired flux level is maintained even at low speeds. As a result, the speed response (Fig. 8(a)) becomes stable with minimal oscillation, and the slip (Fig. 8(b)) is smooth and well-regulated. These results demonstrate that R_s estimation alone is insufficient at very low speeds. Voltage drop compensation is essential to preserve flux accuracy, stabilize the estimation process, and ensure reliable operation.

This paper has been accepted for publication in the AEE journal. This is the version, which has not been fully edited and content may change prior to final publication. Citation information: DOI 10.24425/aee.2026.1991

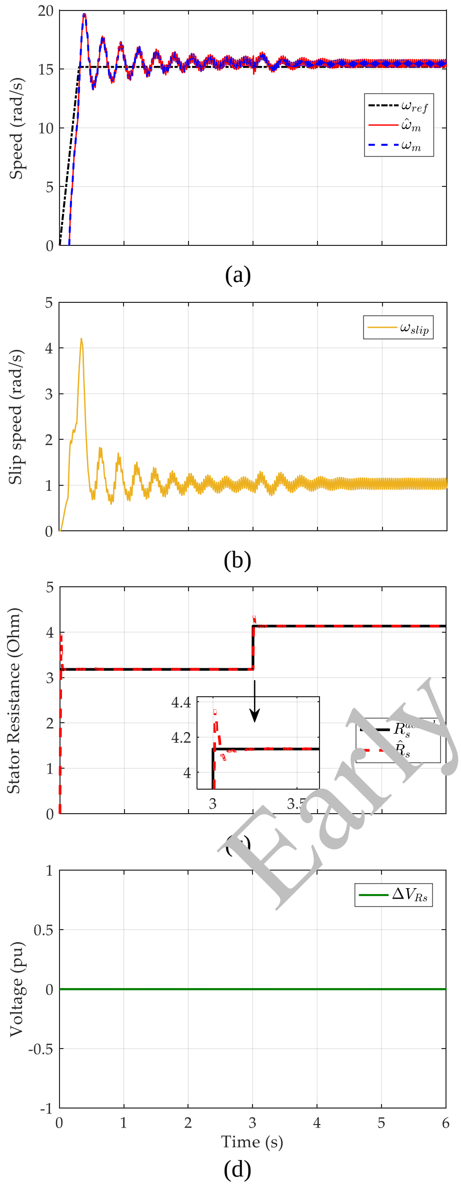

Fig. 7. The results with Method 1 in Scenario 2: (a) speed response; (b) slip speed response; (c) stator resistance response; (d) voltage drop compensation

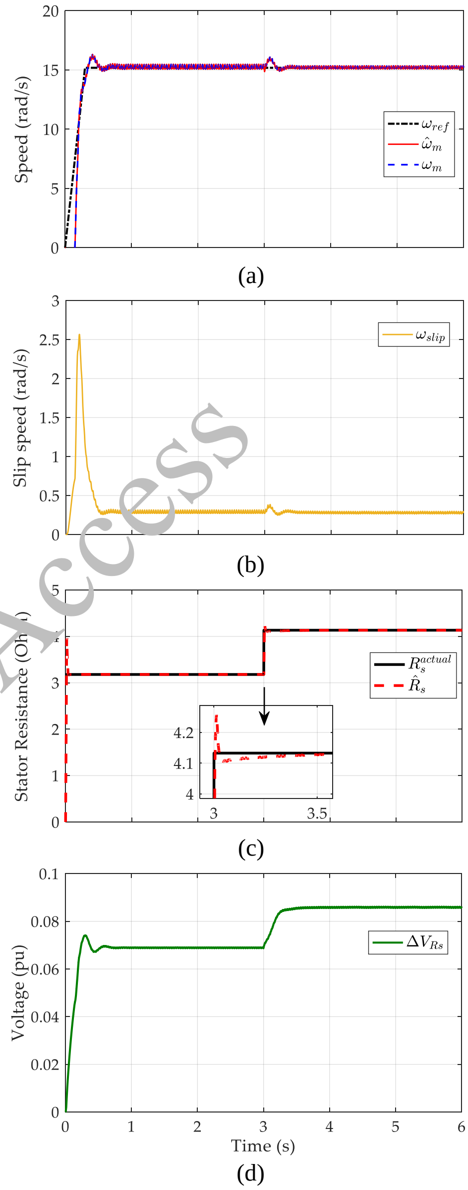

Fig. 8.The results with Method 2 in Scenario 2: (a) speed response; (b) slip speed response; (c) stator resistance response; (d) voltage drop compensation

Scenario 3: Effect of gradual stator resistance variation and stator resistance voltage drop at very low speed.

This paper has been accepted for publication in the AEE journal. This is the version, which has not been fully edited and content may change prior to final publication. Citation information: DOI 10.24425/aee.2026.1991

Scenario 3 evaluates the proposed Method 2 under a gradual stator resistance variation at very low speed. The motor is operated at approximately 15 rad/s, while the stator resistance is increased progressively from its nominal value to about 150% of the rated value. As shown in Fig. 9(a) the measured speed remains close to the reference speed across variations in resistance. Only a brief overshoot occurs during the startup interval, after which the response becomes well damped and stable.

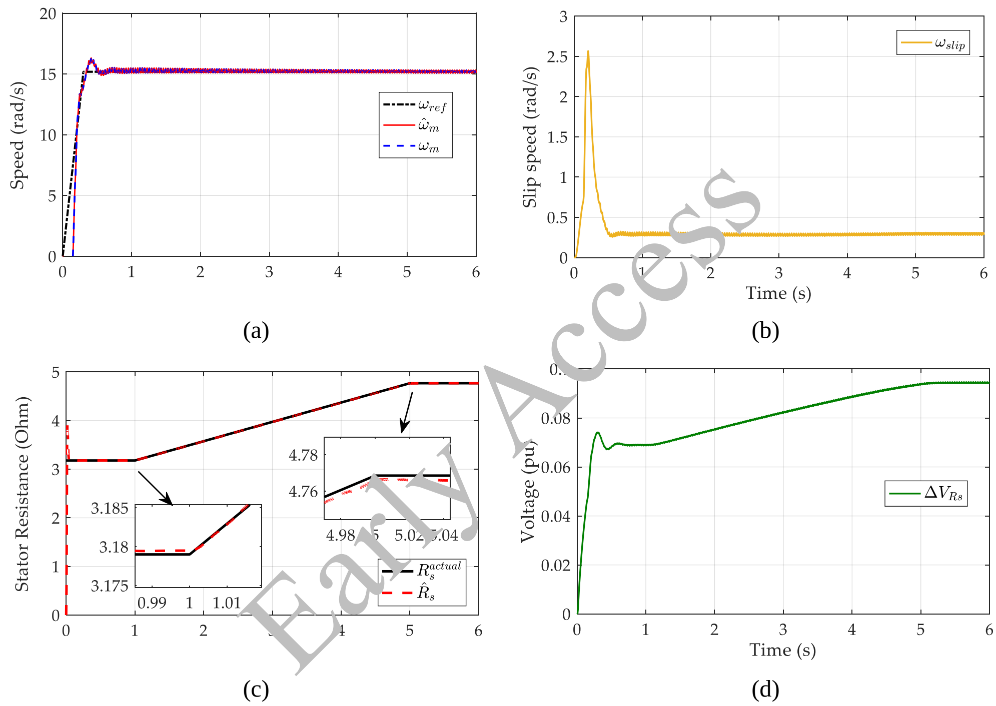

Fig. 9. The results with Method 2 in Scenario 3: (a) speed response; (b) slip speed response; (c) stator resistance response; (d) voltage drop compensation

The slip response in Fig. 9(b) also remains smooth after the initial transient, indicating that the resistance drift does not distort the compensation frequency. In Fig. 9(c), the estimated stator resistance follows the actual resistance with a small delay and a minor steady deviation during the ramp interval. Figure 9(d) shows that the voltage compensation term increases gradually with the estimated resistance and then stabilizes below the imposed limit. Therefore, the combined R_s estimation and voltage compensation mechanism maintains adequate stator flux support at very low speeds without causing instability.

Scenario 4: Wide-speed operation and dynamic performance

Scenario 4 evaluates the robustness of the proposed method (M2) across a wide operating range, including dynamic speed commands and parameter variations. The reference speed profile

This paper has been accepted for publication in the AEE journal. This is the version, which has not been fully edited and content may change prior to final publication.
Citation information: DOI 10.24425/aee.2026.1991

spans multiple regions, including low, medium, and high speeds, with successive acceleration and deceleration phases (Fig. 10(a)), allowing comprehensive assessment of both transient and steady-state performance. The slip response (Fig. 10(b)) shows that slip is continuously adjusted in response to operating conditions. During transients, temporary overshoots occur as the control system increases slip to generate sufficient electromagnetic torque for acceleration or reduces it during deceleration. These overshoots are well damped and converge quickly, indicating stable, responsive dynamic behavior. To further evaluate robustness, the stator resistance is varied during operation, increasing by 15% at t = 3 s and 25% at t = 4.2 s. As shown in Fig. 10(c), the RF-MRAS estimator accurately tracks these changes, maintaining consistency between the internal model and the actual motor. Consequently, the voltage compensation term (Fig. 10(d)) is continuously updated based on the estimated R_s and stator current, ensuring proper flux regulation, particularly at low speeds.

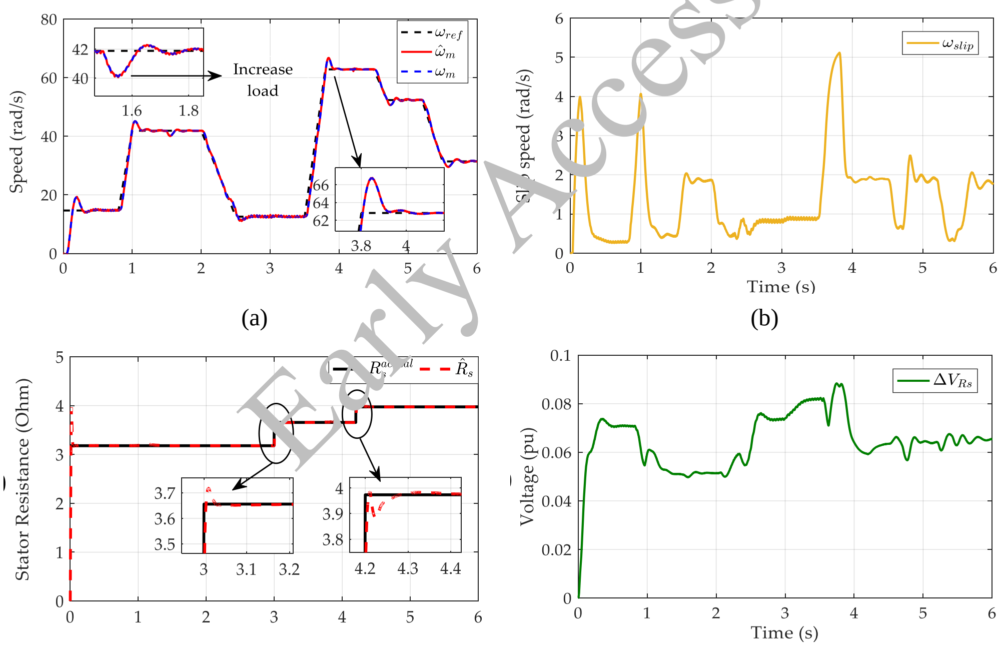

Fig. 10. The results with Method 2 in Scenario 4: (a) speed response; (b) slip speed response; (c) stator resistance response; (d) voltage drop compensation

The stability of the proposed method is further validated through phase-plane and energy-based analyses. The rotor flux error trajectory (Fig. 11(a)) converges to the origin, indicating stable error dynamics, while the flux trajectory in the (α, β) plane (Fig. 11(b)) remains smooth and well-formed. Additionally, the Lyapunov-like energy function (Fig. 11(c)) decreases

This paper has been accepted for publication in the AEE journal. This is the version, which has not been fully edited and content may change prior to final publication.
Citation information: DOI 10.24425/aee.2026.1991

monotonically, confirming bounded and convergent behavior. This is supported by the rapid decay of the flux error (Fig. 11(d)).

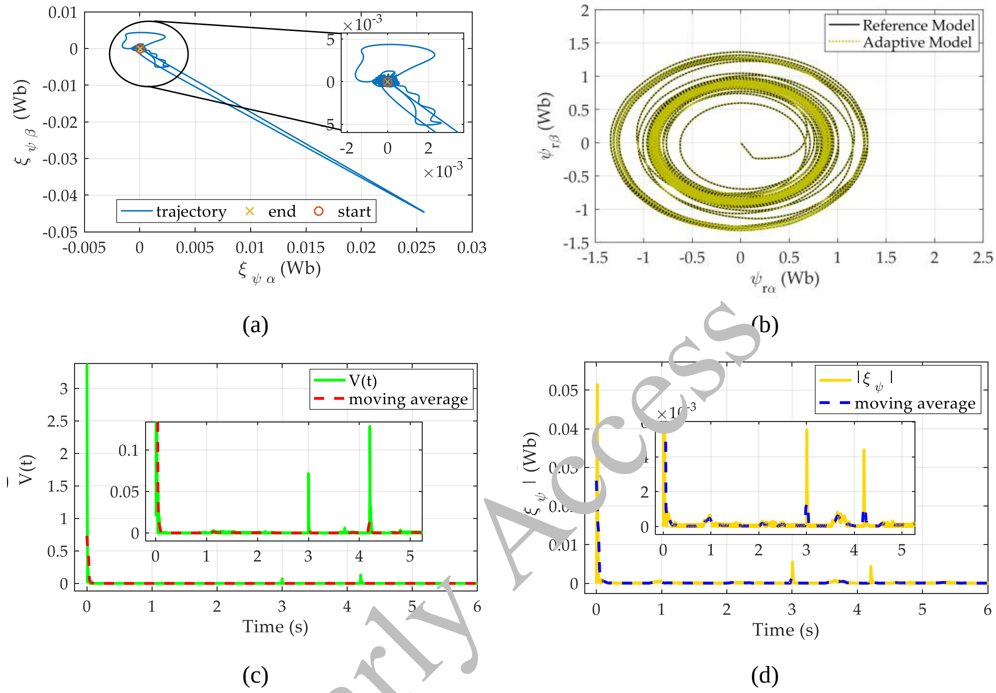

Fig. 11. The stability evaluation with Method 2 in Scenario 4: (a) phase portrait of flux error; (b) rotor flux trajectory; (c) Lyapunov-like energy function; (d) rotor flux error convergence

Scenario 5: Minimum stable speed evaluation

Scenario 5 investigates the minimum achievable operating speed of the induction motor under the three control methods (M0, M1, and M2) using the quantitative criteria defined by E_{MAPE} and $E_{\max}$.

The evaluation is carried out under different load conditions, specifically at T_L = 20%T_{rated}, T_L = 25%T_{rated}, and T_L = 30%T_{rated}, as shown in Figs. (12), (13).

This paper has been accepted for publication in the AEE journal. This is the version, which has not been fully edited and content may change prior to final publication. Citation information: DOI 10.24425/aee.2026.1991

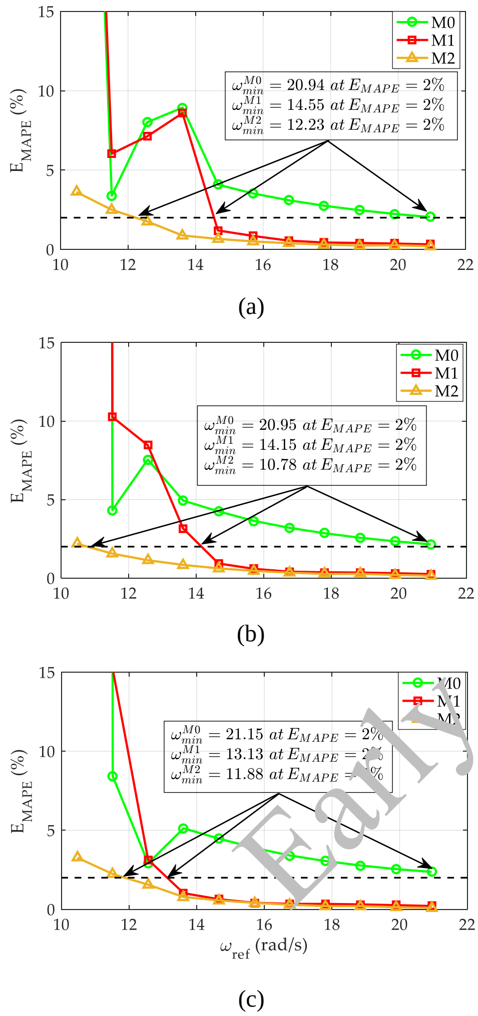

Fig. 12. E_{MAPE} - based evaluation of minimum speed: (a) at $T_L = 20\% T_{\mathrm{rated}}$; (b) at $T_L = 25\% T_{\mathrm{rated}}$; (c) at $T_L = 30\% T_{\mathrm{rated}}$

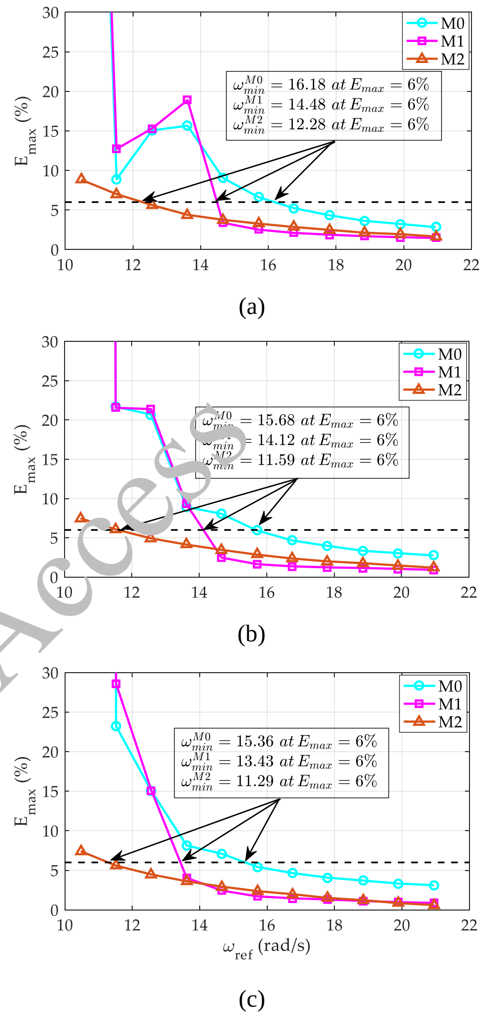

Fig. 13. $E_{\max}$ - based evaluation of minimum speed: (a) At $T_L = 20\% T_{\mathrm{rated}}$; (b) at $T_L = 25\% T_{\mathrm{rated}}$; (c) at $T_L = 30\% T_{\mathrm{rated}}$

For each case, the minimum speed is determined as the lowest reference speed at which both conditions $E_{\max} \leq 6\%$ are simultaneously satisfied. At $T_L = 20\% T_{\mathrm{rated}}$, Fig. 12(a) shows that, based on the E_{MAPE} criterion, the minimum achievable speed is 20.94 rad/s for M0, 14.55 rad/s for M1, and 12.23 rad/s for M2. A similar trend is confirmed in Fig. 13(a) using the $E_{\max}$ criterion, where the corresponding values are 16.18 rad/s (M0), 14.48 rad/s (M1), and 12.28 rad/s (M2). These results indicate that M0 requires a significantly higher minimum speed to maintain stability, whereas M2 achieves the lowest minimum speed among all methods.

This paper has been accepted for publication in the AEE journal. This is the version, which has not been fully edited and content may change prior to final publication.
Citation information: DOI 10.24425/aee.2026.1991

This behavior becomes more pronounced at $T_L = 25\%T_{\text{rated}}$, as illustrated in Figs. 12(b) and 13(b). From Fig. 12(b), the minimum speed according to E_{MAPE} is 20.95 rad/s for M0, 14.15 rad/s for M1, and only 10.78 rad/s for M2. In Fig. 13(b), the $E_{\max}$ - based values are 15.68 rad/s (M0), 14.12 rad/s (M1), and 11.59 rad/s (M2). The reduction achieved by M2 is particularly significant in this case, demonstrating its ability to sustain stable operation at much lower speeds compared to M0 and M1. At a higher load level of $T_L = 30\%T_{\text{rated}}$, the same pattern persists. As shown in Fig. 12(c), the minimum speeds based on E_{MAPE} are 21.15 rad/s for M0, 13.13 rad/s for M1, and 11.88 rad/s for M2. Meanwhile, Fig. 13(c) indicates that the corresponding values based on $E_{\max}$ are 15.36 rad/s (M0), 13.43 rad/s (M1), and 11.29 rad/s (M2). Although the load torque increases, M2 consistently maintains the lowest $\omega_{\min}$, confirming its robustness under more demanding conditions.

The corresponding minimum achievable speeds under each operating condition and evaluation criterion are summarized in Table 4.

Table 4. Minimum achievable speed under different load conditions

Load condition	$T_L = 20\%T_{\text{rated}}$			$T_L = 25\%T_{\text{rated}}$			$T_L = 30\%T_{\text{rated}}$		
Method	M0	M1	M2	M0	M1	M2	M0	M1	M2
$\omega_{\min}$ (rad/s) ($E_{\text{MAPE}} \leq 2\%$)	20.94	14.55	12.23	20.95	14.15	10.78	21.15	13.13	11.88
$\omega_{\min}$ (rad/s) ($E_{\max} \leq 6\%$)	16.18	14.48	12.28	15.68	14.12	11.59	15.36	13.43	11.29

Method M1 improves the situation by incorporating online stator resistance estimation. This reduces modeling error and allows the system to operate at lower speeds than M0. However, as observed in all figures, the improvement is limited. The remaining discrepancy is mainly due to unaccounted stator resistance voltage drop, which still causes flux weakening at low speed. In contrast, Method M2 achieves the best performance in all cases. By combining R_s estimation with real-time voltage drop compensation, the applied stator voltage is effectively corrected. This ensures that the air-gap flux is maintained properly even at very low operating speeds.

7. Experiments

The proposed control scheme was further evaluated on a laboratory induction motor drive platform (Fig. 14). The setup includes a three-phase induction motor coupled to a controllable load machine, with separate voltage-source inverters for the motor and load sides. A TMS320F28335 digital signal controller drives the motor inverter, and the control algorithm is implemented in C++ using Code Composer Studio.

This paper has been accepted for publication in the AEE journal. This is the version, which has not been fully edited and content may change prior to final publication. Citation information: DOI 10.24425/aee.2026.1991

Two experimental tests were carried out. In the first test, the motor was operated at 300 rpm, and an external stator resistance was inserted to emulate a 20% increase in R_s. The responses with and without online R_s estimation were compared. In the second test, the reference speed was reduced to 50 rpm, where the stator voltage drop becomes more critical. With R_s estimation kept active, the drive performance was examined without and with stator voltage compensation.

In the first experimental scenario, the stator resistance mismatch causes a clear degradation when R_s estimation is not used. As shown in Fig. 15, both the estimated and measured speeds exhibit sustained oscillations around the 300 rpm reference, indicating that the RF-MRAS model without R_s adaptation is no longer well matched to the real motor. After enabling online R_s estimation, Fig. 16 shows a much better response.

The speed rises smoothly, the steady-state ripple is significantly reduced, and the measured speed remains close to the reference. The results from Fig. 16 confirm that R_s adaptation improves the flux model accuracy and increases the robustness of the sensorless scalar drive under stator resistance variation.

At 50 rpm, the benefit of voltage compensation becomes more evident. Although R_s estimation is active in both tests, Fig. 17 shows that the drive cannot maintain the reference speed when the stator voltage drop is not compensated. The measured speed settles far below 50 rpm, with persistent oscillations, because the available stator voltage is insufficient to sustain the required air-gap flux. After adding voltage compensation, the response in Fig. 18 is markedly improved. A transient overshoot appears at startup, but the speed then converges close to the reference and remains stable in steady state. The compensation term is necessary to restore the effective stator voltage at very low speed in the scalar control method.

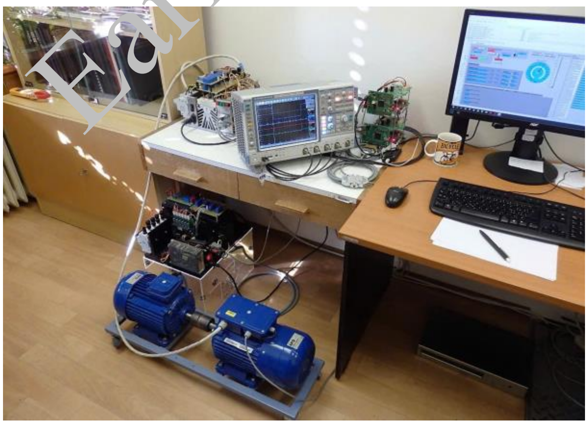

Fig. 14. Laboratory stand

This paper has been accepted for publication in the AEE journal. This is the version, which has not been fully edited and content may change prior to final publication. Citation information: DOI 10.24425/aee.2026.1991

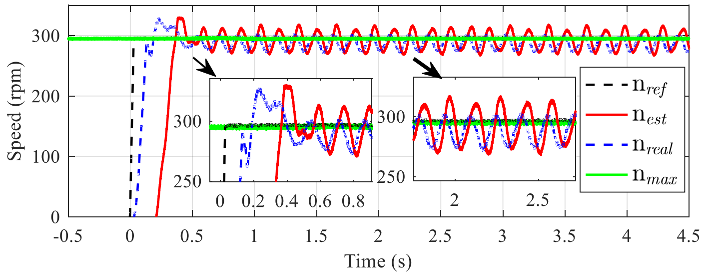

Fig. 15. Experimental results at 300 rpm (without R_s estimation)

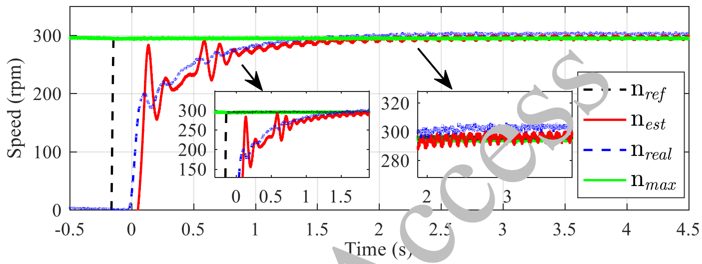

Fig. 16. Experimental results at 300 rpm (with R_s estimation)

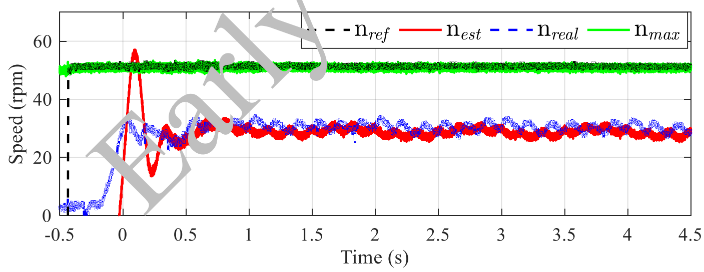

Fig. 17. Experimental results at 50 rpm (with R_s estimation + without voltage compensation)

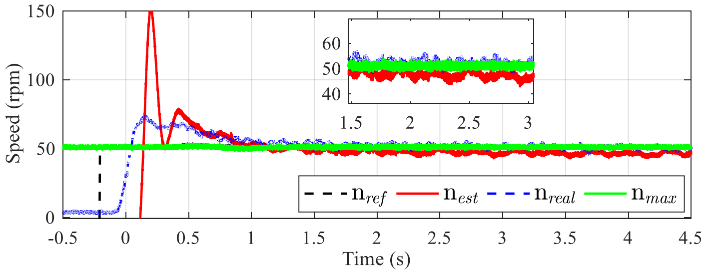

Fig. 18. Experimental results at 50 rpm (with R_s estimation + with voltage compensation)

8. Conclusions

This paper has presented an enhanced sensorless scalar control scheme for induction motor drives based on a dual RF-MRAS framework. By combining rotor speed estimation, stator resistance adaptation, and stator voltage drop compensation, the proposed method improves low-speed operation while preserving the simplicity of conventional V/f control. Simulation results confirmed better speed tracking and a lower minimum stable operating speed under different load conditions and stator resistance variations. Experimental tests further supported these findings. At 300 rpm, online R_s estimation reduced speed oscillations when the stator resistance was increased by 20%. At 50 rpm, voltage compensation restored the effective stator voltage and improved tracking performance at very low speeds. The experimental validation was limited to a 20% increase in Rs due *to* hardware constraints; the 50% variation was examined only in simulation. Future work will extend the hardware tests to larger resistance changes and investigate the integration of the proposed dual RF-MRAS structure into FOC and DTC-based drives.

Acknowledgements

This research is funded by Ton Duc Thang University and by VSB-Technical University of Ostrava.

References

[1] Mohammadi F., Bok R., *Real-time controller-hardware-in-the-loop testing of DC motor-drive systems*, Advances in Electrical and Electronic Engineering, vol. 22, no. 1 (2024), DOI: 10.15598/aeee.v22i1.5720.

[2] Vyas D., Morawiec M., Ayana T., Wogi L., Guziński J., *Active flux based adaptive and non-adaptive observer for sensorless interior permanent magnet synchronous machine drive*, Archives of Electrical Engineering, vol. 73, no. 3 (2024), DOI: 10.24425/aee.2024.150896.

[3] Tran C.D., Kuchar M., Sotola V., Nguyen P.D., *Sensor fault diagnosis strategy based on rotor flux observers in three-phase induction motor drive*, Scientific Reports, vol. 16, no. 267 (2026), DOI: 10.1038/s41598-025-29381-9.

[4] Wang K., Li Y., Ge Q., Shi L., *An improved indirect field-oriented control scheme for linear induction motor traction drives*, IEEE Transactions on Industrial Electronics, vol. 65, no. 12, pp. 9928–9937 (2018), DOI: 10.1109/TIE.2018.2815940.

[5] Elnaggar M.F., Flah A., El-Bayeh C.Z., Alrashed M.M., *Optimized FOC control strategy for dual stators permanent magnet machine*, Scientific Reports, vol. 15, no. 1, 34010 (2025), DOI: 10.1038/s41598-025-11435-7.

[6] Kondratenko D., Lewicki A., Łuksza K., *Augmented speed control scheme of dual induction motors with mutual flux angle control loop*, Archives of Electrical Engineering, vol. 72, no. 4, pp. 915–930 (2023), DOI: 10.24425/aee.2023.147418.

[7] Boukhalfa G., Belkacem S., Chikhi A., Benaggoune S., *Direct torque control of dual star induction motor using a fuzzy-PSO hybrid approach*, Applied Computing and Informatics, vol. 18, no. 1–2, pp. 74–89 (2022), DOI: 10.1016/j.aci.2018.09.001.

[8] Muduli U.R., Behera R.K., Al Hosani K., El Moursi M.S., *Direct torque control with constant switching frequency for three-to-five phase direct matrix converter fed five-phase induction motor*

drive, IEEE Transactions on Power Electronics, vol. 37, no. 9, pp. 11019–11033 (2022), DOI: 10.1109/TPEL.2022.3167477.

[9] Oh G.-U., Hong C.-W., Ko J.-S., *Sensorless speed control in induction motor using deadbeat discrete flux observer under V/f control*, Energies, vol. 18, no. 18, 4934 (2025), DOI: 10.3390/en18184934.

[10] Travieso-Torres J.C., Vilaragut-Llanes M., Costa-Montiel Á., Duarte-Mermoud M.A., Aguila-Camacho N., Contreras-Jara C., Álvarez-Gracia A., *New adaptive high starting torque scalar control scheme for induction motors based on passivity*, Energies, vol. 13, no. 5, 1276 (2020), DOI: 10.3390/en13051276.

[11] Travieso-Torres J.C., Duarte-Mermoud M.A., *Normalized model reference adaptive control applied to high starting torque scalar control scheme for induction motors*, Energies, vol. 15, no. 10, 3606 (2022), DOI: 10.3390/en15103606.

[12] dos Santos T.H., Goedtel A., da Silva S.A.O., Suetake M., *Scalar control of an induction motor using a neural sensorless technique*, Electric Power Systems Research, vol. 108, pp. 322–330 (2014), DOI: 10.1016/j.epsr.2013.11.020.

[13] Ctibor J., Pazdera I., *Comparison of the common control techniques of induction machines*, IEEE International Conference on Environment and Electrical Engineering and IEEE Industrial and Commercial Power Systems Europe (EEEIC/I&CPS Europe), Palermo, Italy, pp. 1–6 (2018), DOI: 10.1109/EEEIC.2018.8494497.

[14] Awdaa M.A., Obed A.A., Yaqoob S.J., *A comparative study between V/F and IFOC control for three-phase induction motor drives*, IOP Conference Series: Materials Science and Engineering, 012006 (2021), DOI: 10.1088/1757-899X/1105/1/012006.

[15] Brandstetter P., Kuchar M., *Sensorless control of variable speed induction motor drive using RBF neural network*, Journal of Applied Logic, vol. 24, pp. 97–108 (2017), DOI: 10.1016/j.jal.2016.11.017.

[16] Bekhiti B., Fragulis G.F., Hariche K., Sharkawy A.N., *Artificial intelligence-enhanced sensorless vector control of induction motors using adaptive neuro-fuzzy systems: experimental validation and benchmark analysis*, International Journal of Robotics and Control Systems, vol. 5, pp. 1828–1849 (2025), DOI: 10.31763/ijrcs.v5i3.1950.

[17] El Daoudi S., Lazrak L., El Ouanjli N., Ait Lafkih M., *Sensorless fuzzy direct torque control of induction motor with sliding mode speed controller*, Computers and Electrical Engineering, vol. 96, 107490 (2021), DOI: 10.1016/j.compeleceng.2021.107490.

[18] Benlaloui I., Chrifi-Alaoui L., Ouriagli M., Khemis A., Khamari D., Drid S., *Improvement of the induction motor sensorless control based on the type-2 fuzzy logic*, Electrical Engineering, vol. 103, no. 3, pp. 1473–1482 (2021), DOI: 10.1007/s00202-020-01178-1.

[19] Orlowska-Kowalska T., Dybkowski M., *Stator-current-based MRAS estimator for a wide range speed-sensorless induction-motor drive*, IEEE Transactions on Industrial Electronics, vol. 57, no. 4, pp. 1296–1308 (2009), DOI: 10.1109/TIE.2009.2031134.

[20] Dinh B., Tran C., Kuchar M., Nguyen P., *Enhanced rotor slip compensation method based on synchronous speed model for scalar control in induction motor drives*, International Review of Electrical Engineering (IREE), vol. 20, no. 4, pp. 296–302 (2025), DOI: 10.15866/iree.v20i4.27006.

[21] Kubatko M., Bielesz D., Kirschner S., Hamani K., Kuchar M., Mrovec T., Prazenica M., *Sensorless direct field-oriented control of induction motor drive using artificial neural network-based reactive power MRAS*, Sensors, vol. 25, no. 23, 7135 (2025), DOI: 10.3390/s25237135.

[22] Saifi R., *Implementation of a new flux rotor based on model reference adaptive system for sensorless direct torque control modified for induction motor*, Electrical Engineering and Electromechanics, no. 2, pp. 37–42 (2023), DOI: 10.20998/2074-272X.2023.2.06.

[23] Ji Juan, Cui Y., Wang K., *Speed sensorless adaptive rotor flux orientation control of induction motor drive*, Authorea (2023), DOI: 10.22541/au.169686035.54584096/v1.

[24] Diop M., Kebe A., Gueye I., *Evaluation of sensorless VF-MRAS and FOC-MRAS of IM electrical drive system*, International Journal of Applied Power Engineering, vol. 14, no. 3, pp. 513–521 (2025), DOI: 10.11591/ijape.v14.i3.pp513-521.

[25] Zhou M., Cheng S., Feng Y., Xu W., Wang L., Cai W., *Full-order terminal sliding-mode-based sensorless control of induction motor with gain adaptation*, IEEE Journal of Emerging and Selected Topics in Power Electronics, vol. 10, no. 2, pp. 1978–1991 (2021), DOI: 10.1109/JESTPE.2021.3081863.

[26] Wogi L., Morawiec M., Ayana T., *Sensorless control of induction motor based on super-twisting sliding mode observer with speed convergence improvement*, IEEE Access, vol. 12, pp. 74239–74250 (2024), DOI: 10.1109/ACCESS.2024.3404040.

[27] Mossa M.A., Echeikh H., Iqbal A., Duc Do T., Al-Sumaiti A.S., *A novel sensorless control for multiphase induction motor drives based on singularly perturbed sliding mode observer-experimental validation*, Applied Sciences, vol. 10, no. 8, 2776 (2020), DOI: 10.3390/app10082776.

[28] Bach D., Tran C., *An improved voltage model based on stator resistance estimation for FOC technique in the induction motor drive*, Advances in Electrical and Electronic Engineering, vol. 22, no. 2, 107 (2024), DOI: 10.15598/aeee.v22i2.5745.

[29] Bednarz S.A., Dybkowski M., *Estimation of the induction motor stator and rotor resistance using active and reactive power based model reference adaptive system estimator*, Applied Sciences, vol. 9, no. 23, 5145 (2019), DOI: 10.3390/app9235145.

[30] Khan Y.A., Verma V., *Stator resistance estimation for MRAS-based speed sensorless vector-controlled switched reluctance motor drive*, Electrical Engineering, vol. 103, no. 4, pp. 1949–1963 (2021), DOI: 10.1007/s00202-020-01203-3.

[31] Badini S.S., Verma V., *A new stator resistance estimation technique for vector-controlled PMSM drive*, IEEE Transactions on Industry Applications, vol. 56, no. 6, pp. 6536–6545 (2020), DOI: 10.1109/TIA.2020.3025265.

[32] Kojabadi H.M., Abarzadeh M., Farouji S.A., *Robust stator resistance identification of an IM drive using model reference adaptive system*, Energy Conversion and Management, vol. 65, pp. 507–517 (2013), DOI: 10.1016/j.enconman.2012.06.020.

[33] Luo H., Wang Q., Deng X., Wan S., *A novel V/f scalar controlled induction motor drives with compensation based on decoupled stator current*, IEEE International Conference on Industrial Technology, Mumbai, India, pp. 1989–1994 (2006), DOI: 10.1109/ICIT.2006.372556.

[34] Zhang Z., Bazzi A.M., *Robust sensorless scalar control of induction motor drives with torque capability enhancement at low speeds*, IEEE International Electric Machines and Drives Conference (IEMDC), San Diego, CA, USA, pp. 1706–1710 (2019), DOI: 10.1109/IEMDC.2019.8785159.

[35] Tran C.D., Truong M.N., *Sensorless control for induction motor drive applying CB-MRAS integrating stator resistance estimation*, International Review on Modelling and Simulations (IREMOS), vol. 17, no. 4, pp. 215–221 (2024), DOI: 10.15866/iremos.v17i4.24107.

[36] Jedryczka C., Stepien S., Demenko A., Nowakowski M., *Infinite-time optimal feedback control of a 3-phase asynchronous motor exploiting a nonlinear finite element model*, Archives of Electrical Engineering, vol. 73, no. 4, pp. 927–939 (2024), DOI: 10.24425/aee.2024.152103.

[37] Tran C.D., Kuchar M., Nguyen P.D., *Improved speed sensorless control for induction motor drives using rotor flux angle estimation*, Electrical Engineering and Electromechanics, no. 6, pp. 93–97 (2025), DOI: 10.20998/2074-272X.2025.6.12.

[38] Brandstetter P., Kuchar M., *Rotor flux estimation using voltage model of induction motor*, International Scientific Conference on Electric Power Engineering (EPE), Kouty nad Desnou, Czech Republic, pp. 246–250 (2015), DOI: 10.1109/EPE.2015.7161090.

[39] Phan T.T., Tran C.D., *A slip compensation technique based on improved current-based model reference adaptive system for scalar control method*, Electrica, vol. 26, 0165 (2026), DOI: https://doi.org/10.5152/electrica.2026.25165.